Applied Catalysis B: Environmental 163 (2015) 382–392

Contents lists available at ScienceDirect

Applied Catalysis B: Environmental

journal homepage: www.elsevier.com/locate/apcatb

Global kinetic modeling of hydrothermal aging of NH_3-SCR over Cu-zeolites

Supriyanto[a], Kurnia Wijayanti[a], Ashok Kumar[b], Saurabh Joshi[b], Krishna Kamasamudram[b], Neal W. Currier[b], Aleksey Yezerets[b], Louise Olsson[a,*]

[a] Chemical Engineering, Competence Centre for Catalysis, Chalmers University of Technology, SE-412 96 Göteborg, Sweden
[b] Cummins Inc., 1900 McKinley Avenue, MC 50183, Columbus, IN 47201, USA

ARTICLE INFO

Article history:
Received 21 March 2014
Received in revised form 21 July 2014
Accepted 25 July 2014
Available online 18 August 2014

Keywords:
Kinetic model
Hydrothermal aging
Ammonia SCR
Cu/BEA
Cu zeolites

ABSTRACT

In this study, a kinetic model describing the effect of hydrothermal aging (at 500, 600, 700, 800 and 900 °C) on Cu-zeolites is developed. The model accounts for the impact of hydrothermal aging on key reactions such as ammonia adsorption/desorption, NH_3 oxidation, NO oxidation, standard SCR, rapid SCR, and NO_2 SCR. In addition, a mechanism for the complex N_2O formation were developed. The effect of aging on ammonia adsorption and desorption were established using micro-calorimeter data. Thereafter, an aging factor model was developed containing two aging factors, one related to over-exchanged copper sites and the other to under-exchanged copper sites. This approach worked well for ammonia and NO oxidation up to an aging temperature of 800 °C, whereas for the SCR reactions only to 700 °C. According to UV–vis, fresh and mildly aged catalysts are dominated by copper hydroxyls, while after aging at high temperature copper oxides are observed. We therefore introduce one SCR reaction associated with copper oxides, simultaneously with one SCR reaction associated with ion-exchanged Cu sites and the updated model could describe the experimental findings well. The results from the model also suggest that the standard SCR reaction is more deactivated during aging compared to SCR with NO_2 present in the feed. After the 900 °C aging the BEA structure had collapsed, resulting in that several parameters in the model needed to be retuned. The results from this modeling study clearly show how complex the hydro thermal aging is over copper zeolites.

1. Introduction

Ammonia based selective catalytic reduction (SCR) is an important technology for reducing NO_x emissions from diesel and lean burn gasoline vehicles. In several of the after-treatment systems vanadia supported on titania [1–5] were used but over the past years, research on ion-exchanged zeolites have been dominating. In particular, copper [6–14] and iron [15–17] exchanged zeolites have received large attention. There are several differences between copper and iron, e.g., copper-zeolites show higher low temperature activity compared to Fe-zeolites [18]. Cu-zeolites also exhibit higher ammonia storage and ammonia oxidation at lower temperature as compared to Fe-zeolites [19]. Several different types of zeolites, ion-exchanged with copper have been reported in literature, for example Cu-faujasite [20], Cu-ZSM-5 [21–24], Cu-BEA [19,25] and Cu-Y [26]. Recently, copper-zeolites and silicoaluminophosphate with chabazite (CHA) structure, like Cu-SAPO-34 [27] and Cu-SSZ-13 [28], have shown promising properties due to their high thermal stability and hydrocarbon resistance [28].

In an after-treatment system, the SCR catalyst might be placed after a diesel particulate filter (DPF). During DPF regeneration it is possible that the temperature in the SCR catalyst is increased and this is one reason for that it is important to examine the hydro thermal aging of the SCR catalyst. In addition, accelerated hydrothermal aging at high temperatures is a method to simulate long-term hydrothermal aging at lower temperatures. For example, according to Schmieg et al. [28] laboratory aging for 16 h at 800 °C agrees well with a catalyst aged in vehicle for 135,000 miles. The effect of hydrothermal aging have been examined for several NH_3-SCR catalysts, including Cu-BEA [19,29–31], Cu-ZSM-5 [8,29], Cu-CHA [28], Fe-BEA [29,32,33], Fe-FER [34] and Fe-MOR [34]. Iwasaki et al. [34] examined the hydrothermal stability of several different Fe-ion-exchanged zeolites and observed that the aging characteristic depends on the zeolite type. However, the comparison was difficult since different zeolites exhibited different particle sizes and

* Corresponding author. Tel.: +46 31 772 4390; fax: +46 31 772 3035.
E-mail address: louise.olsson@chalmers.se (L. Olsson).

http://dx.doi.org/10.1016/j.apcatb.2014.07.059
0926-3373/

Nomenclature

A_i	pre-exponential factor for reaction i ($m^{-1}\ s^{-1}$)
c_k	mole fraction at the reaction layer of species k (−)
c_k^B	mole fraction in the gas bulk of species k (−)
d_{hyd}	hydraulic diameter of the channel (m)
$D_{k,g}$	diffusion coefficient of species k in the gas mixture
$E_{A,i}$	activation energy for reaction i (J/mol)
GSA	geometric surface area per reactor volume (m^{-1})
ΔH	heat of adsorption (kJ/mol)
$k_{k,m}$	mass transfer coefficient of species k (mol/(m^2 s))
k_i	rate constant for reaction i ($m^{-1}\ s^{-1}$)
$MG_{k,G}$	molar mass of gas phase species k (kg/kmol)
r_i	reaction rate for reaction i (kmol/(s m^3))
R	gas constant (J/(mol K))
ΔS	entropy change (J/(mol K))
T_S	temperature at catalyst surface (K)
t	time (s)
$v_{k,i}$	stoichiometric coefficient of species k in reaction i (−)
$w_{k,g}$	mass fraction of species k in gas phase (−)
z	spatial coordinate in axial direction (m)

Greek letters

$\alpha_{k,i}$	coverage dependence for species k in reaction i (−)
ε_g	volume fraction of gas phase in entire system (−)
θ_k	coverage of specie k (−)
ρ_g	density of the gas phase (kmol/m^3)
Ψ_j	surface site density of storage site j (kmol/m^2)

since zeolites with small crystallites showed higher rate of deterioration. Schmieg et al. [35] examined the aging of Cu-CHA and observed that the NO_x conversion during SCR were significantly decreased after 3 h aging at 900 °C. Further, they proposed that such severe aging causes zeolite collapse and Cu agglomeration. Cheng et al. [36] examined the aging behavior of supplier Cu/zeolites and observed that a combination of urea and hydrothermal aging is much more severe compared to hydrothermal aging alone [36]. In earlier studies we examined the hydrothermal aging of Cu-BEA in detail and used those experimental investigations [19,30,31] form the basis for the kinetic model presented in this paper. We observed that for fresh and mildly aged catalyst the copper was in the form of copper hydroxyls as shown by UV–vis, whereas after hydrothermal aging at 800 and 900 °C, copper in the form of copper oxides was detected [31]. Further, material balances using hydrogen consumption in TPR data showed an excellent agreement for the transition of all copper species from Cu^{2+} to Cu^0 during reduction [30]. In addition the zeolite structure collapsed after aging at high temperature (900 °C), as could be seen in XRD [31]. The aging severely affected both ammonia storage as well as SCR activity [19].

Kinetic models for NH_3-SCR have been developed for several catalysts, including vanadia on titania [1–5], Cu-ZSM-5 [21–24], Cu-faujasite [20], HZSM-5 [37] and Fe-zeolites [15–17,38]. Both detailed [22–24] as well as global kinetic models [13,21,39] for NH_3-SCR over copper-zeolites are presented in the literature. In a kinetic model of NH_3-SCR, it is crucial to describe the ammonia storage and release properly; parameters for this can be determined by micro-calorimetry, which has been presented in a study by Wilken et al. [25]. Other important reaction steps are NO oxidation [14], ammonia oxidation and standard SCR [21,40,41]. In order to increase the reaction rate of the SCR, it is beneficial to use equal amounts of NO and NO_2 and it is, therefore, crucial in a kinetic model to also include reaction steps for fast SCR and NO_2 SCR [21]. In addition, N_2O production is significant for many copper-zeolites, such as, for example, Cu-ZSM-5 and Cu-BEA [19]. There are very few aging models for NH_3-SCR available in the literature. Shwan et al. [32] have presented an aging model for Fe-BEA, that describes ammonia storage, NO oxidation and standard SCR. However, there are no kinetic models that describe the effect of hydrothermal aging on rapid and slow SCR reactions. In addition, to our knowledge there are no kinetic models available that describes aging of copper-zeolites used for NH_3-SCR.

The objective of this study is to develop a kinetic model that describes the effect of hydrothermal aging on NH_3-SCR over copper zeolites. The model also describes the effect of aging on SCR with a varying NO_2 to NO_x ratio. In addition, the mechanism for N_2O production was further developed in order to capture the experimental behavior.

2. Experimental

The catalyst and experiments used when developing this model are described in detail in an earlier publication [19]. BEA zeolite, from Zeolyst International, with a silica to alumina ratio of 38, was used as starting material for preparing Cu-BEA [19]. The Cu content was determined using ICP-AES, which resulted in 4 wt% [19]. Monolith samples for Cu-BEA were prepared by incipient wetness impregnation using Boehmite as a binder and 400 cpsi cordierite substrate [19]. Initially, a thin alumina layer was applied to the monolith in order to increase the attachment of the zeolite layer. The prepared monolith catalyst samples had the dimension of 21 mm in diameter and 20 mm in length.

The activity of the catalyst was measured in a flow reactor, which consists of a quartz tube surrounded by a heating coil. The gases were controlled by mass flow controllers (Bronkhorst) and the water flow by a CEM-system (Controlled Evaporation Mixer system from Bronkhorst). The temperature in the gas phase was used for controlling the temperature in the experiments, whereas the temperature measured in the center of the monolith was used in the simulations. The outlet gases were analyzed using an FTIR (MKS MultiGas 2030 HS FTIR). Argon was used as an inert carrier gas and the total flow was 3500 ml/min, which yields a space velocity of 30,300 h^{-1}. Initially, the catalyst was degreened using 8% O_2, 5% H_2O and 5% CO_2 for 3 h, followed by 2 h with 400 ppm NH_3, 400 ppm NO, 8%O_2, 5% H_2O and 5% CO_2 at 500 °C. Prior to each experiment, the sample was pretreated with 8% O_2 at 500 °C for 15 min, in order to remove any residues of ammonia from the surface. After each aging, six experiments were conducted: (i) ammonia temperature programmed desorption (TPD), (ii) ammonia oxidation, (iii) NO oxidation, (iv) standard SCR, (v) rapid SCR using 50% NO_2 and (vi) SCR using 75% NO_2. After each set of experiments the catalyst was aged using 8% O_2, 5% H_2O and 5% CO_2 for 3 h at 600, 700, 800 and 900 °C, respectively [19].

During the ammonia TPD, the catalyst was exposed to 400 ppm NH_3, 5% H_2O and 5% CO_2 at 150 °C. Thereafter, the catalyst was flushed with 5% H_2O and 5% CO_2, followed by a temperature ramp in the same gas mixture to 500 °C at a rate of 10 °C/min. The ammonia oxidation was examined using 400 ppm NH_3, 5% H_2O, 5% CO_2 and 8% O_2 and increasing the temperature stepwise (150, 200, 250, 300, 400 and 500 °C). A similar experiment was conducted for investigating the NO oxidation. Finally, three SCR experiments were conducted using 0, 50 and 75% NO_2 to NO_x ratio. The catalyst was exposed to the gas mixture; 400 ppm NH_3, 400 ppm NO_x, 8% O_2, 5% H_2O, 5% CO_2. Also for these experiments, the temperature was increased stepwise (150, 200, 250, 300, 400 and 500 °C).

3. Kinetic modeling

3.1. Reactor model

A commercial software, AVL BOOST [42] was used together with user defined files in FORTRAN to perform the kinetic modeling. It was assumed that all channels were uniform and simulations were therefore conducted over one channel, which was discretized into 15 grid points.

The main governing equation for the gas phase species is:

$$\varepsilon_g \frac{\partial \rho_g \cdot w_{k,g}}{\partial t} = \varepsilon_g \frac{\partial \rho_g \cdot w_{k,g} \cdot v_g}{\partial z} + MG_{k,g} \sum_i^{nr} v_{i,k} \cdot r_i(c_k, T_s, \theta_k) \quad (1)$$

and for the coverage of component k on the surface:

$$\frac{\partial \theta_k}{\partial t}(\Theta \cdot GSA) = \sum_i^{nr} v_{i,k} \cdot r_i(c_k, T_s, \theta_k) \quad (2)$$

where, the geometric surface area per unit reactor volume, GSA, is given by:

$$\frac{GSA}{d_{hyd}} = 4 \times (\text{cell density}) \quad (3)$$

Further, the film model was used to describe the mass transport from the gas bulk to the surface, according to:

$$GSA \cdot k_{k,m} \cdot (c_k - c_k^B) = \sum_i^{nr} v_{i,k} \cdot r_i(c_k, T_s, \theta_k) \quad (4)$$

where, the mass transfer coefficient $k_{k,m}$ is determined by the correlation with *Sh* number:

$$k_{k,m} = \frac{sh \cdot D_{k,g}}{d_{hyd}} \quad (5)$$

The Sherwood number is calculated according to the Sieder/Tate correlation. The mass transport in the washcoat was neglected, which also have been done in several other modeling studies of NH_3-SCR [15,17,21]. In order to minimize mass transport resistance, we intentionally used a thin washcoat. In addition, in an earlier study by Olsson et al. [21], the mass transport resistance in the wash-coat of Cu-ZSM-5 was examined by using a second monolith with an 11 wt% washcoat compared to the usual 23 wt%. Simultaneously, the total flow was reduced in half. The same conversion during standard SCR was observed during the entire temperature interval (100–500 °C), which indicates that there are no mass-transport limitations in the washcoat. It should be mentioned that at higher temperatures (250–500 °C), complete conversion of the ammonia was obtained; thus, at these temperatures, the results are inconclusive. Therefore, it cannot be ruled out that there is some influence from mass-transfer in the wash-coat at higher temperatures and the kinetic parameters received should be treated as apparent rate parameters. Further, small zeolite particles (about 1 μm according to SEM [25]) have been used in the synthesis in order to minimize the internal diffusion in the particles.

The heat balance was not solved owing to the fact that the heat associated with NH_3-SCR is low in combination with very low feed concentrations, an approach that has been used in several previous models [6,17,21–24]. The temperature measured in the catalyst was used in the simulation.

3.2. Kinetic model

The rate constants are determined using the Arrhenius equation, according to

$$k_i = A_i e^{-E_{A,i}/(RT_S)} \quad (6)$$

Ammonia is stored in significant amounts over zeolites [7,18,28,43], something that is also the case for ion-exchanged zeolites, e.g., Cu-BEA [19,25]. In order to capture the transient effects of NH_3-SCR over Cu-zeolites, it is therefore crucial to arrive at a good description of the ammonia storage and release. Previously, we developed a method using micro-calorimetry at atmospheric pressure to determine the coverage-dependent heat of adsorption [25]. The heat of adsorption is in an excellent agreement with the Temkin isotherm, which has been used in several kinetic models to describe ammonia adsorption and desorption during SCR reaction [5,16,21,24,44]. It is common to assume that the adsorption is non-activated [45], which results in the following form describing the activation barrier for ammonia desorption

$$E_{\text{desoption},NH_3} = E^0_{\text{desoption},NH_3}(1 - \alpha\theta_{NH_3-S1}) \quad (7)$$

The ammonia adsorption has previously been described both by single site models [21] and more detailed multiple sites models [17,24,46,47]. The main reason for adding a second or additional sites to a model is to describe the ammonia loosely bound at low temperatures. For kinetic models valid from 150 °C and higher, one adsorption site has been found to be sufficient in previous studies [21]. Ammonia may adsorb on different sites in a zeolite. Wang et al. [48] examined the ammonia adsorption on Cu-SAPO-34 using DRIFT spectroscopy and found that ammonia adsorbs in the form of NH^{4+} on Brönstedt acid sites and NH_3 on the Lewis sites. The Lewis sites are predominately the copper sites. Ammonia adsorption on both Lewis and Brönstedt acid sites were also observed over Cu-SSZ-13 [49] using DRIFT spectroscopy. In addition using TPD in the DRIFT reactor, Wang et al. [48] found that the desorption profiles were analogous for both ammonia on the Lewis and Brönstedt sites from 200 °C, which suggest that the binding strength were similar. This is in line with earlier studies, where the TPD profile after ammonia adsorption were similar for H-BEA as well as Cu/BEA [50] and in the same way for H-ZSM-5 and Cu-ZSM-5 [24]. To conclude ammonia adsorbs on both Brönstedt and Lewis acid sites, likely with similar strength. In order to simplify the model we have, therefore, chosen to use only one adsorption site and micro-calorimeter data for the coverage-dependent heat of adsorption after degreening/aging at 500, 600, 700 and 780 °C [19]. The reactions and corresponding rates are shown in Table 1.

Furthermore, at high temperature, ammonia oxidation occurs and produces predominately N_2 (NO, NO_2, NH_3, and N_2O are measured by the FTIR), which is shown in Reaction (R2) (Table 1). A large dataset was used to develop the rate expression and it was found that a reaction order for oxygen lower than one was needed in order to describe the experimental features occurring when varying the oxygen concentration. However, small amounts of N_2O were also produced (less than 10 ppm), which was why Reaction (R3) was added. NO formation during ammonia oxidation was not observed for fresh and aged catalysts up to 800 °C, but after aging at 900 °C, non-zero amount of NO was observed and for this specific case, Reaction (R4) was added. The same reaction order for oxygen was used for all three ammonia oxidation reactions. Further, an additional reaction for NO oxidation to NO_2 was also incorporated in the model, which is shown in Reaction (R5) (Table 1). A global reaction was used between NO and oxygen in the gas phase. However, this does not mean that the reaction proceed in gas phase, this is only

Table 1
Reactions and rates for ammonia storage, ammonia oxidation and NO oxidation.

Reaction		Reaction rate
$NH_3 + S1 \overset{r_1}{\leftrightarrow} NH_3 - S1$	(R1)	$r_1 = \Psi(k_{1,f} C_{NH_3} \theta_{S1} - k_{1,b} \theta_{NH_3-S1})$
$4NH_3 - S1 + 3O_2 \overset{r_2}{\rightarrow} 2N_2 + 6H_2O + 4S1$	(R2)	$r_2 = \Psi k_2 C_{O_2}^{0.6} \theta_{NH_3-S1}$
$4NH_3 - S1 + 4O_2 \overset{r_3}{\rightarrow} 2N_2O + 6H_2O + 4S1$	(R3)	$r_3 = \Psi k_3 C_{O_2}^{0.6} \theta_{NH_3-S1}$
$4NH_3 - S1 + 5O_2 \overset{r_4}{\rightarrow} 4NO + 6H_2O + 4S1$ [a]	(R4)	$r_4 = \Psi k_4 C_{O_2}^{0.6} \theta_{NH_3-S1}$
$NO + 0.5O_2 \overset{r_5}{\leftrightarrow} NO_2$	(R5)	$r_5 = \Psi(k_{5,f} C_{O_2}^{0.5} C_{NO} - k_{5,b} C_{NO_2})$

[a] Only used after 900 °C aging.

Table 2
Reactions and rates for ammonia SCR.

Reaction	Reaction rate
$4NH_3 - S1 + 4NO + O_2 \xrightarrow{r_6} 4N_2 + 6H_2O + 4S1$ (R6)	$r_6 = \Psi k_6 C_{NO} C_{O_2}^{0.5} \theta_{NH_3-S1}$
$2NH_3 - S1 + NO + NO_2 \xrightarrow{r_7} 2N_2 + 3H_2O + 2S1$ (R7)	$r_7 = \Psi k_7 C_{NO} C_{NO_2} \theta_{NH_3-S1}$
$4NH_3 - S1 + 3NO_2 \xrightarrow{r_8} 3.5N_2 + 6H_2O + 4S1$ (R8)	$r_8 = \Psi k_8 C_{NO_2} \theta_{NH_3-S1}$

a simplification in the model. This type of reaction for NO oxidation have been used in other studies, for both copper [21] and iron zeolites [17]. Further, in the reaction rate the site density (Ψ) is included and in this way is the rate depending on the amount of sites. The site density is added to all reaction rates.

Furthermore three irreversible reactions covering the standard SCR, rapid SCR and NO_2 SCR were introduced in the kinetic model (Reactions (R6)–(R8)) as shown in Table 2). These reactions have been used in several kinetic models [17,21]. The reaction order for oxygen in the standard SCR was received during the tuning of data with multiple oxygen concentrations (data not shown here).

Large amount of N_2O formation was observed at low temperature and thereafter its formation decreased with increasing temperature. Interestingly, at high temperature, the N_2O production starts to increase again [19,51,52]. In addition, in a study by Wilken et al. [19], it was observed that hydrothermal aging resulted in a decrease of the N_2O formation at low temperature, whereas an increase was visible at high temperature. It is therefore likely that two different routes for producing N_2O exist. Further, when increasing the NO_2 content in the feed, an increased N_2O formation follows [21,51,52]. The formation and decomposition of ammonium nitrate are suggested to be the reason for the N_2O formation at low temperature [50,51]. Further, when exposing Cu-BEA catalysts to NO_2 and NH_3, the formation of ammonium nitrate type of species at low temperature occurred [53] and Mihai et al. [50] observed that the formation was higher at 150 than at 200 °C. In the present kinetic model precursors for ammonium nitrate are reversibly formed from either NO or NO_2, since N_2O formation is observed for both NO and NO_2 in the feed [19,51], and these reactions are shown in Table 3 (Reactions (R9) and (R11)). It is critical that the reactions are reversible, since this will give decreased coverage of these species at higher temperature. The decreased coverage of ammonium nitrate precursors results in a decreased formation of N_2O (Reactions (R10) and (R12)) when increasing the tempeature, which is also observed experimentally [31,50,51]. These reaction steps are in line with the kinetic model presented by Colombo et al. [41], where S-NO_3[NH_3] was used in the detailed mechanism for N_2O formation over commercial Cu-zeolites.

As described above, at high temperature, the N_2O formation starts to increase again and, therefore, two additional reactions for N_2O formation are added (Reactions (R13) and (R14)), for the cases with NO and NO_2 in the feed, respectively. In addition, we previously observed that ammonia can react with NO_2 to produce NO [51] over high-loaded Cu-BEA samples. This reaction was also included in a kinetic model by Watling et al. [54]. We found that for aged samples this reaction became more important and was only included in the model after 900 °C aging (Reaction (R15)).

In addition, after aging at 800 and 900 °C an additional SCR reactions was needed (Reaction (R16)), due to the formation of copper oxides. This is throughly discussed in Section 4.4.

4. Results and discussion

4.1. Ammonia storage and release

Cu-zeolites store ammonia [6,25] and it is therefore crucial to have a good description of the storage and release of ammonia

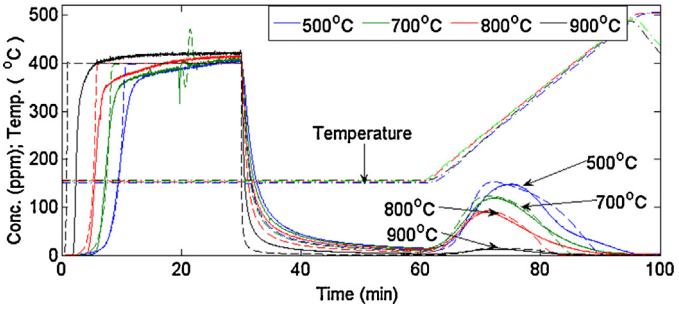

Fig. 1. The effect of hydrothermal aging on ammonia TPD. The experimental results are shown in solid lines and the model in dashed lines for a Cu-BEA catalyst degreened/aged at 500, 700, 800 and 900 °C.

in a kinetic model, in order to capture the transient effects [6]. Consequently, we have developed a procedure for determining coverage-dependent heat of adsorption at atmospheric pressure using micro-calorimetry and the results of applying this method on ammonia over Cu-BEA are shown in [25]. We have also measured the coverage-dependent heat of adsorption for ammonia over 4% Cu-BEA catalysts, which had been degreened/aged at 500, 600, 700 and 780 °C for 3 h using 8% O_2 and 2% H_2O [19]. The reproducibility was examined by repeating the experiment conducted for the powder degreened at 500 °C. The results are given in ref. [19] and shows an excellent reproducibility. It was found that the heat of adsorption decreased slightly with aging temperature (in the aging interval of 500–780 °C); this finding is also in line with the fact that the ammonia desorption peak possessed a small shift toward lower temperatures during ammonia temperature programmed desorption (TPD) experiments [19]. These micro-calorimetry results were used in the model. It was assumed that the aging using 2% (which was the case with the DSC) and 5% water (used in the flow reactor experiments) were similar and the reason for using 2% water in the calorimeter experiments were attributed to the water supply system. Because the calorimeter had a limitation in temperature, we used the results from the 780 °C calorimeter experiment in the simulation at 800 °C. The coverage dependent heat of adsorption used in the model, based on micro-calorimetry data, is presented in Table 4.

Ammonia TPD experiments were used to simulate the adsorption and desorption after different aging temperatures. In these experiments, the catalyst sample was exposed to 400 ppm NH_3, 8% O_2, 5% H_2O and 5% CO_2 at 150 °C after which the sample was flushed with H_2O and CO_2 in Ar and the temperature ramped to 500 °C. The resulting ammonia concentration from both the experiment (solid lines) and simulation (dashed lines) for the Cu-BEA catalyst degreened at 500 °C are shown in Fig. 1. The pre-exponential factors for adsorption and desorption, as well as the number of storage sites, are tuned to the experiment and the values are found in Tables 4 and 5. The model can predict experimental results adequately, which shows that the procedure of using micro-calorimetry in combination with kinetic modeling works well. In order to simulate ammonia storage after different aging temperatures, the micro-calorimetry data were used as described above and the amount of storage sites were fitted to the experiments (Table 4). Due to limitations in temperature for the calorimeter, hydrothermal aging experiment was not performed at 900 °C in the micro-calorimeter and the heat of adsorption was accordingly tuned to the TPD experiment performed on the bench-flow reactor. There was a significant decrease in ammonia storage already after aging at 700 °C and the storage decreased with increasing aging temperature. After 900 °C aging only a minor amount of ammonia storage was observed. After such high aging temperature we

Table 3
Reactions and rates for N_2O formation and NO_2 dissociation and a second SCR reaction.

Reaction		Reaction rate
$NH_3 - S1 + NO \overset{r_9}{\leftrightarrow} S1 - NH_3 - NO$	(R9)	$r_9 = \Psi(k_{9f} C_{NO} \theta_{NH_3-S1} \theta_{S1} - k_{9b} \theta_{S1-NH_3-NO})$
$2S1 - NH_3 - NO + O_2 \overset{r_{10}}{\rightarrow} N_2O + N_2 + 3H_2O + 2S1$	(R10)	$r_{10} = \Psi k_{10} C_{O_2} \theta_{S1-NH_3-NO} \theta_{S1}$
$NH_3 - S1 + NO_2 \overset{r_{11}}{\leftrightarrow} S1 - NH_3 - NO_2$	(R11)	$r_{11} = \Psi(k_{11f} C_{NO_2} \theta_{NH_3-S1} \theta_{S1} - k_{11b} \theta_{S1-NH_3-NO_2})$
$2S1 - NH_3 - NO_2 \overset{r_{12}}{\rightarrow} N_2O + N_2 + 3H_2O + 2S1$	(R12)	$r_{12} = \Psi k_{12} \frac{\theta_{S1-NH_3-NO_2} \theta_{S1}}{1+K_{inhib,12} \theta_{S1-NH_3-NO_2}}$
$2NH_3 - S1 + 2NO + O_2 \overset{r_{13}}{\rightarrow} N_2O + N_2 + 3H_2O + 2S1$	(R13)	$r_{13} = \Psi k_{13} C_{NO} C_{O_2} \theta_{NH_3-S1}$
$2NH_3 - S1 + 2NO_2 \overset{r_{14}}{\rightarrow} N_2 + N_2O + 3H_2O + 2S1$	(R14)	$r_{14} = \Psi k_{14} C_{NO_2} \theta_{NH_3-S1}$
$2NH_3 - S1 + 3NO_2 \overset{r_{15}}{\rightarrow} 3NO + N_2 + 3H_2O + 2S1$	(R15)	$r_{15} = \Psi k_{15} C_{NO_2} \theta_{NH_3-S1}$
$4NH_3 - S1 + 4NO + O_2 \overset{r_{16}}{\rightarrow} 4N_2 + 6H_2O + 4S1$	(R16) [a]	$r_{16} = \Psi k_{16} C_{NO} C_{0.2}^{0.5} \theta_{NH_3-S1}$

[a] Only used after 800 and 900 °C aging.

Table 4
The surface density and heat of adsorption used in the model after different aging temperatures. Micro-calorimetry data for degreened/aged catalyst at 500, 600, 700 and 780 °C are used.

Parameters	Aging temperature (°C)				
	500	600	700	800	900
Surface density (mol/m^2)[a]	0.0437	0.0396	0.0354	0.0242	0.0030
Heat of adsorption (kJ/mol)	112.75	109.98	107.36	104.40[b]	120.0[c]
α	0.39	0.37	0.35	0.31[b]	0.27[c]

[a] Geometric surface area per unit reactor volume, GSA is 2650 m^2/(m^3 monolith).
[b] Data for aging at 780 °C in micro-calorimeter is used in model for 800 °C.
[c] For 900 °C heat if adsorption is fitted to ammonia TPD.

observed with XRD that the BEA structure collapsed [31], something that explains the low level of ammonia storage.

4.2. Ammonia and NO oxidation

The ammonia oxidation occurs at high temperature and decreases the selectivity for the NO_x reduction [6,19]. In order to predict the ammonia and NO concentration, it is therefore crucial to examine the ammonia oxidation separately and develop a model for this reaction [17,21,24,40]. The resulting NH_3, N_2O and NO concentrations for experiments with NH_3 in the presence of O_2, H_2O, and CO_2 and the stepwise increase in temperature are shown in Fig. 2. At the start of experiment, a large uptake of ammonia was observed due to the large storage capacity and when the temperature is increased stepwise a release of ammonia is seen because of desorption. At 400 °C, NH_3 oxidation starts to occur and the rate is further increased at 500 °C. Small amounts of N_2O are visible at higher temperature (<10 ppm), but NO formation was not observed for the moderately aged cases. However, after severe aging at 900 °C, NO is also observed. It should be noted that after this high temperature aging XRD showed that the zeolite structure was collapsed [31], and a different behavior should therefore be expected.

The ammonia oxidation is modeled by using Reaction (R2) (Table 1) and the parameters for NH_3 storage and release described in Section 4.1 and Table 5. In addition, Reaction (R3) is used for ammonia oxidation that produces N_2O and Reaction (R4) for producing NO (only used after aging at 900 °C). The reaction rates depend on the coverage of ammonia on the sites as well as the oxygen concentration. However, oxygen in the gas phase is used in order to simplify the model, since oxygen storage is not likely important. Further, the site density is included in all reaction rates in order to consider the amount of sites present in the current catalyst.

The results in Fig. 2 show both the experiment and the developed model. First, the pre-exponential factors and activation energies for ammonia oxidation were tuned to the degreened catalyst (denoted 500 °C in Figure) and the parameters given in Table 5. The activation barrier for ammonia oxidation is similar to earlier modeling studies, in which for example, Olsson et al. [21] estimated 162.4 kJ/mol using Cu-ZSM-5 and Metkar et al. [40] 178.8 kJ/mol for Cu-CHA. However, in a study performed after this modeling study, we estimated a lower value for ammonia oxidation over 4% Cu-BEA using Arrhenius plots [50]. Since ammonia oxidation only occurs at high temperature, there are less data to fit the model to, which results in a large correlation between the pre-exponential factor and

Table 5
Parameters for the kinetic model for the degreened catalyst (at 500 °C).

Reaction	Pre-exp. factor (m^{-1} s^{-1})[a]	Activation energy (kJ/mol)	Reaction	Pre-exp. factor (m^{-1} s^{-1})[a]	Activation energy (kJ/mol)
1f. Ammonia adsorption	9.278×10^6	0.0	9f. S1-NH_3-NO formation	8.00×10^5	0.0
1b. Ammonia desorption[b]	6.757×10^{12}	112.75	9b. S1-NH_3-NO dissoc.	5.00×10^{11}	65.0
2. Ammonia oxidation to N_2	1.864×10^{15}	180.0	10. N_2O low temp. from NO	1.59×10^{14}	95.0
3. Ammonia oxidation to N_2O	4.160×10^{15}	205.0	11f. S1-NH_3-NO_2 formation	1.60×10^7	0.0
4. Ammonia oxidation to NO	1.927×10^{16} Only used for 900 °C	215.0	11b. S1-NH_3-NO_2 dissoc.	1.735×10^{15}	95.0
5. NO oxidation[d]	1.439×10^7	48.0 [21]	12. N_2O low temp. from NO_2[c]	6.112×10^{13}	95.0
6. Standard SCR	5.842×10^{13}	84.9 [21]	13. High temp. N_2O from NO	3.311×10^{18}	160.0
7. Rapid SCR	2.826×10^{18}	85.1 [21]	14. High temp. N_2O from NO_2	2.25×10^{15}	120.0
8. NO_2 SCR	1.480×10^{10}	52.0	15. NO formation	Only used for aged samples	

[a] The unit of the reaction rate is mol/(m^3 s), whereas the coverages and concentrations are dimensionless.
[b] $\alpha = 0.39$.
[c] $K_{inhib,12} = 75.0$.
[d] Parameters for forward reaction, backward reaction from thermodynamic equilibrium.

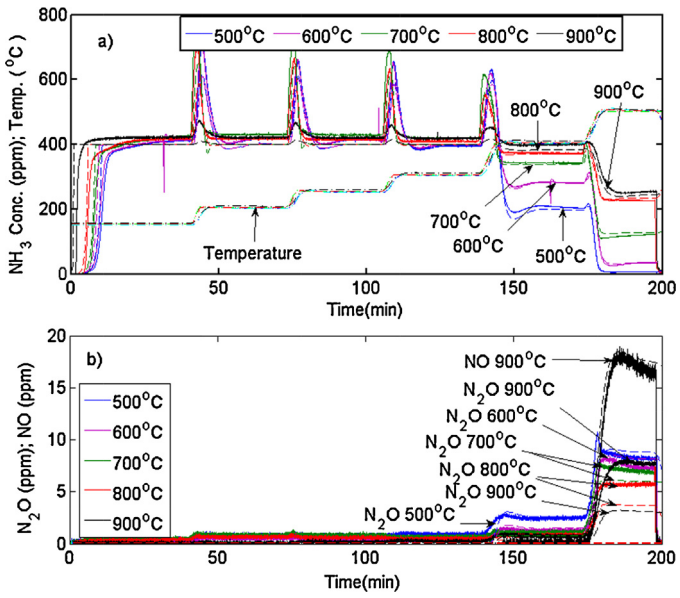

Fig. 2. The effect of aging on ammonia oxidation, where (a) is the NH_3 and (b) the N_2O and NO concentrations. The experimental results are shown in solid lines and the model in dashed lines. The catalyst is exposed to 400 ppm NH_3, 8% O_2, 5% H_2O and 5% CO_2.

activation energy; consequently lowering both the activation energy and pre-exponential factor simultaneously would likely also produce a good fit.

A simplified aging model was developed. The major theoretical base for the modeling approach was an experimental study recently performed in which we examined the effect of different copper loadings in Cu-BEA on the rate for different reactions [50]. We found that the reaction rate for ammonia and NO oxidation was increasing with increasing copper loading [50]. However, the results were completely different for the SCR reaction, where the high-loaded Cu sample exhibited the lowest reaction rate, even though the differences were less for this reaction. In low-loaded Cu samples it is likely that the copper binds to two Al. However, for the over-exchanged sample (the Cu/Al >0.5) also sites where Cu is bond to only one Al, and charged-balanced by an OH-group, is formed. The NO and ammonia oxidation rates are higher for over-exchanged Cu-BEA [50] and we therefore suggest that ammonia and NO oxidation primarily occur over sites where Cu binds to only one Al. Further, the SCR rate were faster for low and medium-exchanged Cu-BEA [50] and we propose that the SCR reaction primarily occurs on sites where one Cu binds to two Al, although it does occur on both types of sites. With these results as a base, we introduce a modeling approach with aging factors. We use two aging factors, Factor 1 for the over-exchanged sites and Factor 2 for the under-exchanged sites. The pre-exponential factor for each reaction has been multiplied by the corresponding aging factor. Since ammonia oxidation is proposed to occur on the over-exchanged sites, the pre-exponential factors for ammonia oxidation (Reactions (R2) and (R3) shown in Table 1) were multiplied by Factor 1. Factor 1 was tuned to the results of the different aging experiments depicted in Fig. 2. The values for Factor 1 after different aging temperatures are shown in Table 6. As mentioned above, after 900 °C aging, the zeolite structure collapsed [31] and a small amount of NO was visible during NH_3 oxidation, as simulated using Reaction (R4) (Table 1). Since this reaction was only used for one case, no aging factor was applied. There was good agreement between the model and experiment (Fig. 2) and it was observed that an aging factor worked well for ammonia oxidation. Further, the deactivation of ammonia oxidation also occurred after mild aging, already after 600 °C.

Table 6
Aging factor for different aging temperatures.

Parameters	Aging temperature (°C)				
	500	600	700	800	900
Aging factor 1	1.00	0.75	0.53	0.50	0.35[a]
Aging factor 2	1.00	1.00	0.85	0.40	0.13

[a] Aging factor 1 of NO oxidation at 900 °C is 6.0.

NO oxidation is another reaction occurring over ion-exchanged zeolites, especially for different Cu-zeolites [6,14,22]. The resulting NO_2 levels after exposing the catalyst to NO in the presence of O_2, H_2O, and CO_2 and stepwise increasing the temperature are shown in Fig. 3. Reaction (R5) in Table 1 is used for modeling the NO oxidation and the activation energy from Olsson et al. [21] is used. The pre-exponential factor is tuned using the data in Fig. 3 for the catalyst degreened at 500 °C and the result is found in Table 5. Since the NO oxidation is assumed to occur predominately on the over-exchanged copper sites, which is also the case for ammonia oxidation, aging Factor 1 is used for NO oxidation as well. Thus, Factor 1 (Table 6), tuned to ammonia oxidation was applied to NO oxidation for the cases with aging at 600, 700 and 800 °C and the results are found in Fig. 3. There was very good agreement between the experiment and the model.

However, after aging at 900 °C the NO oxidation rate is increased and larger NO_2 formation was observed, but simultaneously, the ammonia oxidation slightly decreased. The result was that the same aging factors for ammonia and NO oxidation could not be used after 900 °C aging (see Table 6). Earlier UV–vis studies showed that after 800 and 900 °C aging copper oxides were formed, which coincided with a large drop in BET surface area [31], indicating a collapse of the structure. However, XRD showed a structural collapse only after 900 °C aging, but it should be mentioned that the XRD experiments were performed on aged monoliths, whereas the UV–vis and BET experiments were performed on aged powder [31]. In the earlier study we proposed that the aging might have been suppressed on the monoliths either by the effect of the binder or the conditions during the aging [31]. Since the flow reactor experiments used in this modeling study were conducted on a monolith, the zeolite structure probably collapsed after 900 °C aging and also after severe aging copper oxide particles are formed. We suggest that these copper oxide particles exhibit higher activity for NO oxidation and that this might be the reason for the increased NO_2 concentration. This mechanistic proposal is in line with the study by Pereda-Ayo et al. [55], who concluded that CuO catalyzes the oxidation of NO to NO_2.

To summarize, the method using the same aging factor for NH_3 and NO oxidation works well for aging up to 800 °C, but after aging at 900 °C when the zeolite structure had collapsed different values must be used.

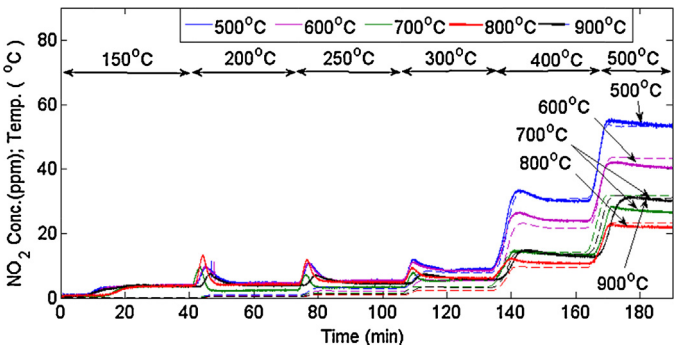

Fig. 3. The effect of aging on NO oxidation. The experimental results are shown by solid lines and the model results in dashed lines. The catalyst was exposed to 400 ppm NO in presence of 8% O_2, 5% H_2O and 5% CO_2.

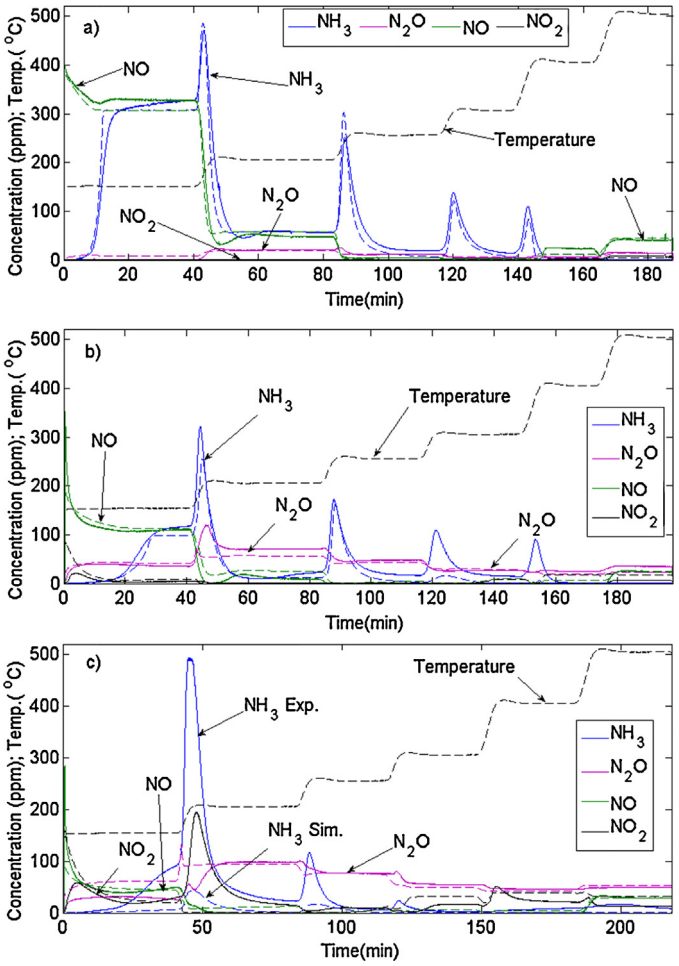

Fig. 4. Experiment (solid lines) and simulation (dashed lines) for SCR with a varying NO_2/NO_x ratio. The NO_2/NO_x ratio is (a) 0, (b) 50% and (c) 75%. The experimental results are given by solid lines and the model results by dashed lines. The catalyst are exposed to 400 ppm NO_x, 400 ppm NH_3, 8% O_2, 5% H_2O and 5% CO_2.

4.3. Ammonia SCR for degreened Cu-BEA

Ammonia SCR experiments with three different NO_2/NO_x ratios (0, 50, 75%) were used to develop the SCR model. The catalyst was exposed to 400 ppm NO_x, 8% O_2, 5% H_2O and 5% CO_2, while increasing the temperature stepwise; the results are shown in Fig. 4. Three reaction steps were added for standard SCR, rapid SCR and NO_2 SCR (Reactions (R6)–(R8)). N_2O formation was observed with a maximum at 200 °C [19] and thereafter declined, but increased again at high temperature. We therefore propose two N_2O routes, one at low temperature (Reactions (R9) and (R10)) and another at high temperature (Reaction (R13)). In previous studies, it was proposed that the low temperature formation of N_2O was associated with the formation of ammonium nitrate species [41,50,51,53]. We have therefore, added the formation and decomposition of ammonium nitrate precursors on the active sites. When increasing the temperature, the coverage of these precursors decreased and this is a crucial feature in order to explain the decrease in N_2O formation when increasing the temperature. This result is in line with the model by Colombo et al. [41], in which S-NO_3[NH_3] species were used in the mechanism for N_2O formation over commercial Cu-zeolites. It is well-known that N_2O formation increased with an increasing amount of NO_2 in the NO_x feed [21,50,51], which is why we have added the corresponding reactions for N_2O production from NO_2 (Reactions (R11), (R12) and (R14)).

In Fig. 4a, the results from the experiment and model for the case with NO in the feed is depicted. NO breaks through directly, when the SCR condition is started, while there is a total uptake of ammonia for an extended period. The reason for this difference is the low storage of NO on the surface and the simultaneous large storage of ammonia. Since the coverage of ammonia is increasing, the reaction rate for standard SCR is also increasing which is the reason for the increase in NO conversion, which the model well describes. When the catalyst is saturated the ammonia breaks through and steady state conditions are obtained. Thereafter, the temperature is increased to 200 °C and the conversion is significantly increased, simultaneously as the N_2O production reaches its maximum. During the temperature ramps, ammonia desorption is visible. At high temperature, the NO concentration is increasing because of the importance of ammonia oxidation (Fig. 2), which results in a deficit of ammonia. The model describes the experimental features well. The model is also developed for fast SCR conditions with the results shown in Fig. 4b. The main differences, compared to the standard SCR case, include the increased activity as well as increased N_2O formation. The model well describes the experimental findings. However, at high temperature, the model under-predicts the release of ammonia when increasing the temperature due to the fact that in the model the stored ammonia is involved in the SCR reactions. Finally, one case with 75% NO_2 is simulated and the experimental and simulated concentrations are shown in Fig. 4c. The model describes the NO and N_2O concentrations adequately, as well as the steady state levels of NO_2 and NH_3. However, when increasing the temperature, the desorbing of NH_3 and NO_2 is under-predicted by the model. Regarding the parameters in the model: (i) the activation energies for the standard and rapid SCR are fixed to literature values [21], (ii) the parameters for ammonia storage and release, NO oxidation and NH_3 oxidation are determined from separate experiments described earlier and (iii) the remaining parameters are manually tuned (Table 5).

4.4. Effect of aging on ammonia SCR

The effect of hydrothermal aging at 500, 600, 700, 800 and 900 °C was examined using experiments with 400 ppm NO_x, 400 ppm NH_3, 8% O_2, 5% H_2O and 5% CO_2 while stepwise increasing the temperature. The resulting NO_x and N_2O concentrations for the case with NO are shown in Fig. 5. Hydrothermal aging at 600 °C has no effect on NO_x conversion, which is interesting considering that the ammonia and NO oxidation was influenced after the aging had occurred (Figs. 2 and 3). These results indicate that these reactions occur on different sites, something that is in line with our earlier study [50], in which we proposed that ammonia and NO oxidation occurs on the over-exchanged Cu sites, while SCR occurs at a faster rate on under-exchanged sites. After 700 °C aging, a clear deactivation is visible, which significantly increases after 800 °C aging. Finally, at 900 °C, the zeolite structure collapses [31], resulting in poor NO_x conversion. The low temperature N_2O formation, related to ammonium nitrate species formation and decomposition [50,51] is decreasing with increasing aging temperature, except for a small difference between 500 and 600 °C aging. Interestingly, at high temperature, the trend is the opposite with increasing N_2O after aging [19], especially after aging at 900 °C where according to XRD the structure collapses [31]. As discussed above, after high temperature aging, copper oxides are observed in UV–vis and may be the reason for the increased NO oxidation activity, the formation of NO during ammonia oxidation and the large effect seen on N_2O formation at high temperature. Indeed, N_2O formation is observed for ammonia SCR over CuO/Al_2O_3 [56], which supports our hypothesis.

Similar trends are found after hydrothermal aging at different temperatures using 50 or 75% NO_2 as NO_x source [19], even though the extent of the deactivation varies. For the fast SCR case

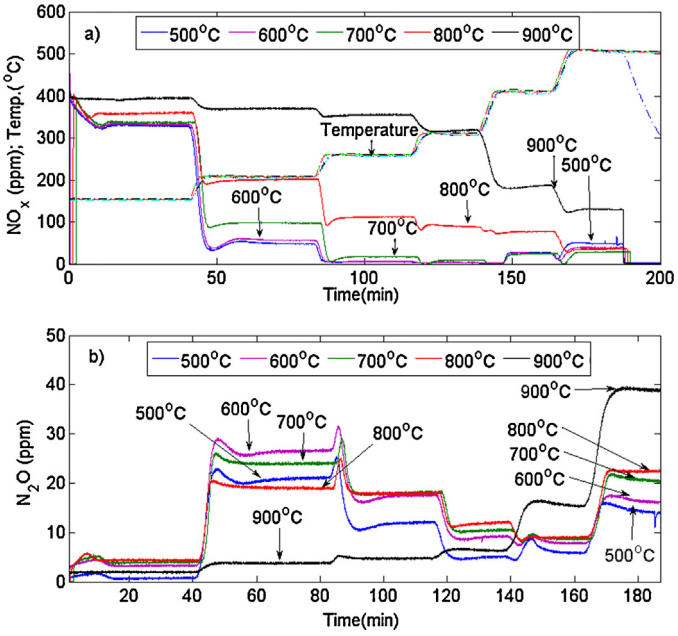

Fig. 5. The effect of aging on SCR with NO_2/NO_x ratio = 0, where (a) is the NO_x and (b) the N_2O concentration. The catalyst are exposed to 400 ppm NO, 400 ppm NH_3, 8% O_2, 5% H_2O and 5% CO_2. The catalyst is degreened/aged at 500, 600, 700, 800 and 900 °C.

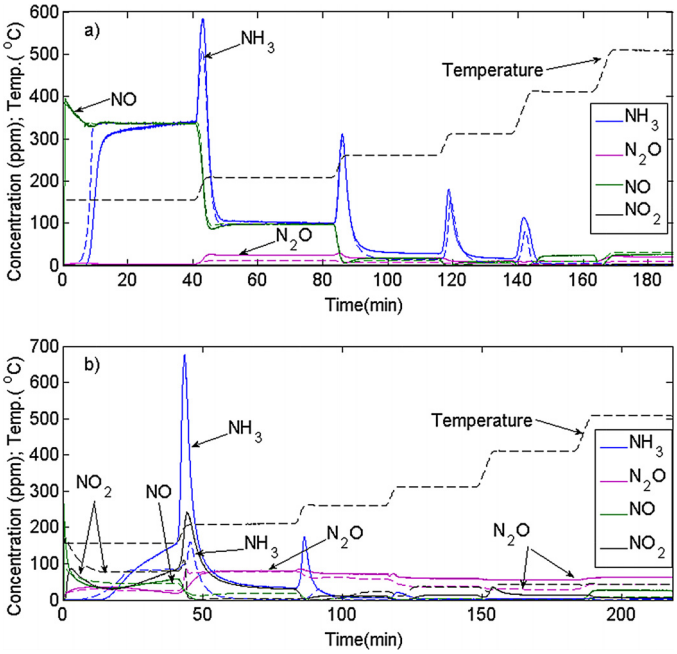

Fig. 6. The effect of aging at 700 °C on the SCR reactions. The experimental results are shown in solid lines and the model results in dashed lines. The catalyst is exposed to 400 ppm NO_x, 400 ppm NH_3, 8% O_2, 5% H_2O and 5% CO_2, where (a) 0% NO_2 and (b) 75% NO_2.

no deactivation is observed after 600 °C aging, but after 800 °C deactivation is visible (no results are available after 700 °C). However, this deactivation is smaller compared to after standard SCR, but the conversion is very high in a large part of the experiment (Fig. 4), which results in that significant deactivation must occur in order to be visible. After 900 °C aging a large deactivation is observed, but it is significantly less compared to the standard SCR case. This is also seen for the 75% NO_2 experiment, where the conversion is even close to 100% at 300 °C. Thus, the SCR rates when using 75% NO_2 is much higher compared to both rapid and standard SCR case after aging at 900 °C. We suggest that the reason for the high NO_2 SCR rates is that they occur on the copper oxides, which are present for severely aged samples.

Since no significant deactivation was observed for the SCR reactions after 600 °C aging, these experiments were therefore not modeled. The aging factor procedure was instead applied on the SCR experiments conducted after aging at 700 °C. Factor 1 was applied on NO and NH_3 oxidation, while Factor 2 was used for the SCR reactions. The N_2O production was significantly higher for the over-exchanged Cu samples. Thus, we propose that these reactions occur on the sites where Cu binds to only one Al, and charged balanced with an OH-group [50,51]. This is the background for applying aging Factor 1 to the N_2O reactions. It is possible that the high temperature N_2O formation occurs on another site, as discussed above, but in order to simplify the model aging Factor1 was also used for this case. Factor 2 was tuned to the standard SCR experiment, and Factor 1 was the same as used for NO and ammonia oxidation (see Table 6). The resulting NO, NO_2, NH_3 and N_2O concentrations from the experiment and model after aging at 700 °C are shown in Fig. 6, where Fig. 6a depicts the results after standard SCR and Fig. 6b shows the results for the 75% NO_2 case. The model well describes the experimental features for the standard SCR case (Fig. 6a). The aging factor approach also works well for the 75% NO_2 case (Fig. 6b); however, the model under-predicts N_2O at high temperature. The reason for the under-prediction is that the high temperature N_2O is increasing with aging [19], possibly due to the CuO formation and since the aging Factor 1 (Table 6) is decreasing with aging, there is an N_2O discrepancy at high temperature.

The hydrothermal aging was also conducted at 800 °C and after exposing the catalyst to 400 ppm NO, 400 ppm NH_3, 8% O_2, 5% H_2O and 5% CO_2 the results of increasing the temperature stepwise are shown in Fig. 7a. In this simulation, aging factors are applied in the same way as after 700 °C aging (Table 6). However, the aging factor model clearly starts to have difficulties in the standard SCR case. The model gives NO and NH_3 concentrations that are to high at low temperature, especially at 200 °C, while significant to low concentrations at high temperature. This simulation is performed with Factor 2 = 0.4. If this factor was increased, a good description of the experiment at low temperature could be obtained; however, the discrepancy at higher temperatures would be even worse. The opposite result would be obtained if Factor 2 was instead decreased. To conclude, the aging factor model does not work well at aging temperature of 800 °C and higher. Clearly, the temperature behavior of the model is not working properly and for this reason we retuned the pre-exponential factor and activation energy for the SCR step (Reaction (R6), Pre-exponential factor: $1.22 \times 10^{10}\ m^{-1}\ s^{-1}$ and activation energy 49.9 kJ/mol, aging factor applied as shown in Table 6). The results of using this model are shown in Fig. 7b. The activation barrier is tuned to get a good agreement at low temperature, which is clearly seen in Fig. 7b. However, the agreement is still poor at high temperature. Thus this modeling approach is not working well.

The reason for why the aging factor model, or even to retune the SCR reaction, did not work well might be that at high aging temperature, other copper species are likely formed. Li et al. [30] characterized the thermal aging of 4% Cu/BEA using H_2-TPR and found that after aging at 800 °C the hydrogen consumption shifted to higher temperature and was broadened. The 900 °C exposure resulted in an even larger change in the TPR profile, with new hydrogen consumption peaks. Li et al. [30] propose that the different peaks are associated with different copper species. In addition, earlier UV–vis experiments showed the formation of copper oxides after hydro thermal aging at high temperature [31]. These results are in line with XANES studies by Kim et al. [57], where increased amount of CuO_x species were found after hydro thermal aging. It

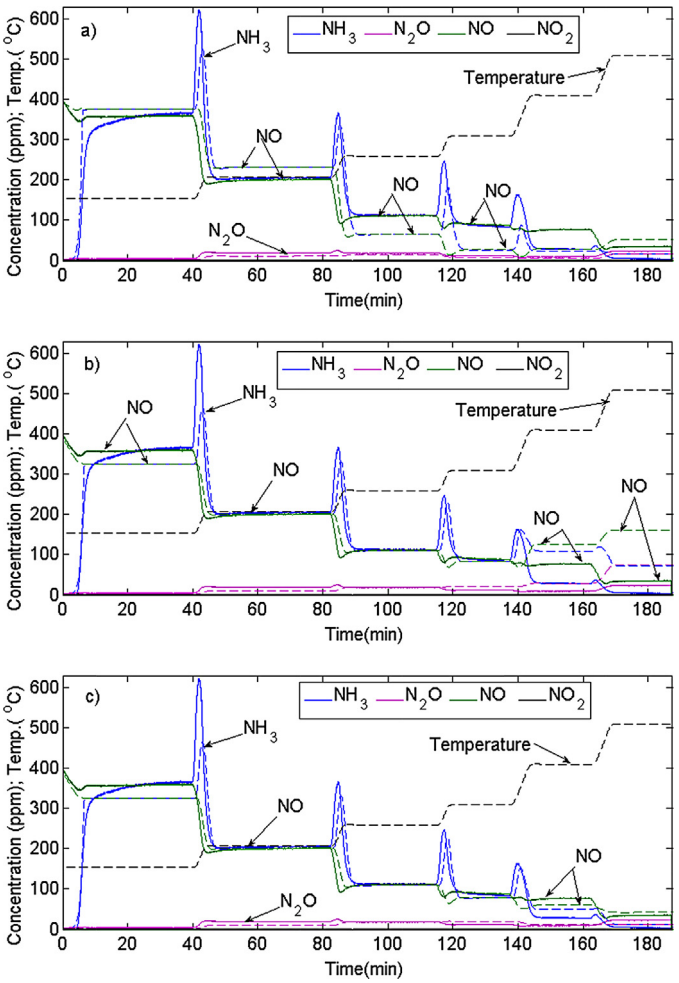

Fig. 7. The effect of aging at 800 °C on the standard SCR using different aging models. The experimental results are shown in solid lines and the model results in dashed lines. The catalyst is exposed to 400 ppm NO, 400 ppm NH_3, 8% O_2, 5% H_2O and 5% CO_2. (a) Using aging factors, (b) using aging factors and retuning the standard SCR reaction and (c) using aging factors, retuning the standard SCR reaction and adding an additional reaction (Reaction (R16)).

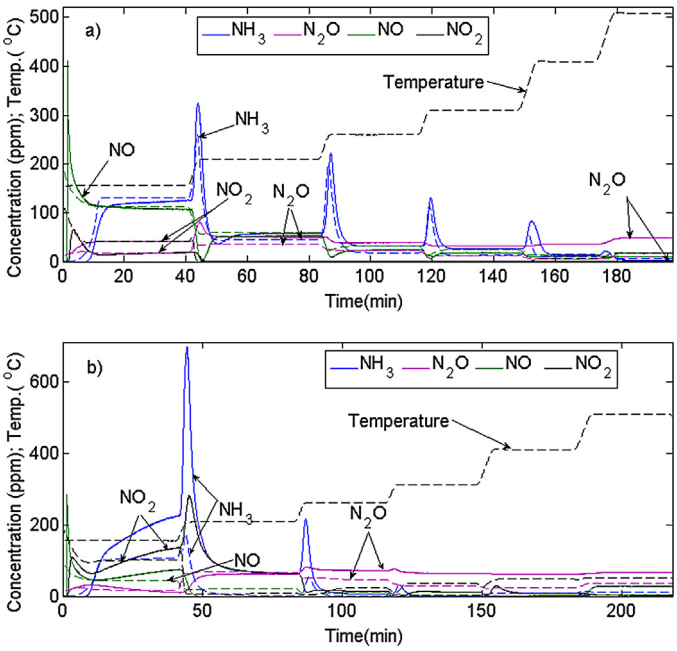

Fig. 8. The effect of aging at 800 °C on the rapid and NO_2 SCR using aging model presented in Fig. 7c and simultaneously aging factor 1.0 for rapid and NO_2 SCR. The experimental results are shown in solid lines and the model results in dashed lines. The catalyst is exposed to 400 ppm NO_x, 400 ppm NH_3, 8% O_2, 5% H_2O and 5% CO_2. (a) 50% NO_2/NO_x ratio and (b) 75% NO_2/NO_x ratio.

has been found that CuO is active for the SCR reaction, for example Pasel et al. [58] observed ammonia SCR activity for CuO supported on active carbon and Xie et al. [59] for CuO/Al_2O_3. Thus, when copper oxides are formed there are two active sites for the SCR reaction, ion-exchanged copper and copper oxides. Accordingly, it is not possible to describe the activity over a large temperature span by using only one SCR reaction. We have therefore added an additional SCR reaction (Reaction (R16)), with the same form of the reaction rate as for Reaction (R6). We suggest that this reaction occurs over copper oxides, but since the ammonia TPD (Fig. 1) shows only one peak it is not possible to determine the number of active sites for each site type. In order to simplify the model, both reactions are therefore modeled on the same site. However, the physical interpretation of adding an extra SCR reaction is that there are two different active sites for the SCR reaction; under-exchanged copper sites and copper oxide sites. Since ion-exchange copper zeolites exhibit good performance at low temperature [6,19], we assume that copper oxides are responsible for the additional activity at high temperature and this is in the model described by using Reaction (R16). The pre-exponential factor and activation energy for Reaction (R16) were tuned to be 3.31×10^{18} m^{-1} s^{-1} and 160.0 kJ/mol, respectively and all other parameters were the same as for the simulation in Fig. 7b. The activation energy was significantly higher for the added SCR reaction because it occurred at higher temperature. The result of this simulation is found in Fig. 7c. The model now describes the experimental results adequately.

The same parameters as were used for the simulation of standard SCR in Fig. 7c were used for simulating fast SCR and NO_2 SCR with 50% and 75% NO_2 to NO_x ratio. However, when applying Factor 2 (which was 0.4 as shown in Table 6) to fast and NO_2 SCR reactions (Reactions (R7) and (R8)), the NO conversion in the simulation was significantly to low. These results clearly show that the rates for standard SCR and fast and NO_2 SCR deactivate with different rates, which is likely because of the fact that they occur on different sites. We also examined the effect of removing the aging factor on fast and NO_2 SCR (Reactions (R7) and (R8)), while keeping all other parameters and reactions as in Fig. 7c and the results are shown in Fig. 8. The model describes the results of fast SCR well, which is depicted in Fig. 8a. But, for the 75% NO_2 case, the conversion in the model was too high at low temperature but with the same aging factors, the 50% NO_2 case was well described. However, the results with the high NO_2 concentration is further complicated by the probable formation of large amount of ammonium nitrate species. Surprisingly, in the simulations the N_2O formation was too low at high temperature when using 75% NO_2, but adequate for the 50% NO_2 case. In the current model, there are two paths for N_2O formation at high temperature, with NO (Reaction (R13)) or NO_2 (Reaction (R14)). However, after aging, the N_2O formation at high temperature seemed to be even more complex. If an N_2O reaction with NO and NO_2 were to be added, a better agreement would likely be retrieved. However, this was omitted in the current simulations in order not to make the model too complex.

The same model as developed for aging at 800 °C, was used applying aging Factor 1 and Factor 2 (Table 6) for describing the SCR activity after 900 °C aging. Note that two different aging factors were used for NO and NH_3 oxidation. After 900 °C aging the zeolite structure completely collapsed, as evidenced by XRD measurements [31]. In addition, after high temperature aging the copper species were shifted from copper hydroxyls to copper oxides, according to UV–vis [31]. We propose that the NO oxidation rate is

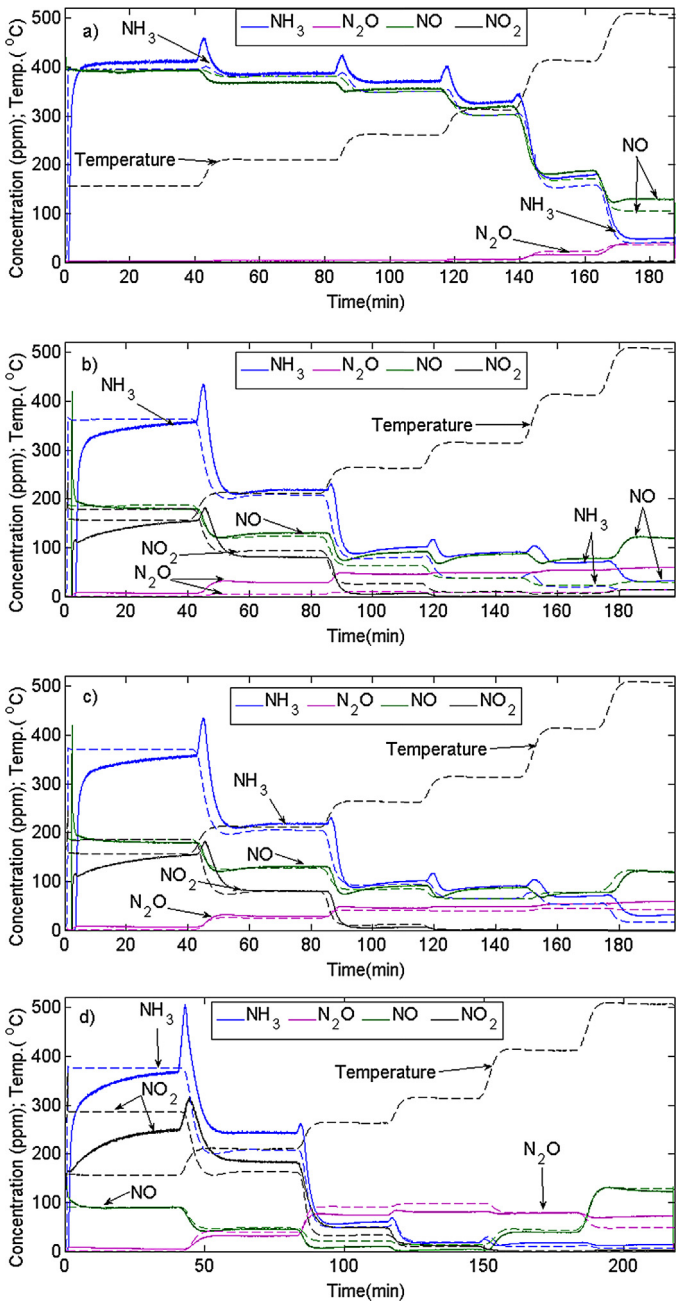

Fig. 9. The effect of aging at 900 °C on the standard, rapid and NO_2 SCR. The experimental results are shown in solid lines and the model in dashed lines. The catalyst is exposed to 400 ppm NO_x, 400 ppm NH_3, 8% O_2, 5% H_2O and 5% CO_2. (a) Standard SCR using aging factors and two SCR steps (b) 50% NO_2, details about the assumptions in the text, (c) 50% NO_2, details about the assumptions in the text (d) 75% NO_2, same model as in (c).

higher on copper oxides, the reason for the increased NO_2 formation during NO oxidation after 900 °C aging compared to after aging at 800 °C, while the ammonia oxidation activity slightly decreased. These results points out the need of different aging factors on NO and NH_3 oxidation after 900 °C aging. The pre-exponential factor for the second SCR rate, interpreted as SCR over copper oxide sites was decreased by a factor of 0.14 from 800 to 900 °C aging, which may be compared to a decrease of 0.325 for the regular SCR reaction. For the rapid and fast SCR reaction (Reactions (R7) and (R8)), the same decrease in pre-exponential factor as for the standard SCR between 800 and 900 °C was applied, giving $A_7 = 9.18 \times 10^{17}\ m^{-1}\ s^{-1}$ and $A_8 = 4.81 \times 10^{9}\ m^{-1}\ s^{-1}$. The resulting simulation for the standard SCR case is depicted in Fig. 9a and as seen the model describes the results adequately.

These parameters were also used for simulating 50% NO_2 to NO_x ratio after 900 °C aging with the results shown in Fig. 9b. The agreement at low temperature for NO, NO_2 and NH_3 is in general good; however, the agreement is poor at high temperature, as well as for N_2O throughout the entire temperature region. The main discrepancy at high temperature is the large amount of NO released in the experiment that had not been predicted by the model. In an earlier study, we observed that significant amounts of NO can be produced from NO_2 [51] over high-loaded Cu-BEA samples, a reaction that was also added in a kinetic model by Watling et al. [54]. For the degreened and midly aged samples, it was not necessary to include this reaction in order to describe the experimental features. However, after the severe aging at 900 °C, this reaction was critical and Reaction (R15) was added, with the parameters $A_{15} = 1.21 \times 10^{22}\ m^{-1}\ s^{-1}$ and $E_{15} = 205.0$ kJ/mol. Experimentally, it is shown that this reaction pre-dominately occurs over "over-exchanged" Cu samples [51] and based on the kinetic modeling development in this study, we propose that this reaction occurs faster on copper oxide sites than on ion-exchanged copper hydroxyles. As described above, the N_2O parameters also needed adjustments ($A_{11f} = 9.6 \times 10^{7}\ m^{-1}\ s^{-1}$, $A_{11b} = 1.04 \times 10^{16}\ m^{-1}\ s^{-1}$, $A_{12} = 3.67 \times 10^{14}\ m^{-1}\ s^{-1}$, $A_{14} = 5.40 \times 10^{16}\ m^{-1}\ s^{-1}$) and in addition, the aging factor for the slow SCR reaction needed to decrease to 0.07. To summarize, large modifications in several parameters relating N_2O formation and NO_2 SCR, in addition to adding an extra step for dissociation of NO_2 to NO, were needed in order to describe the 900 °C aging. It is not surprising that significant changes were needed in the model parameters after this aging since the zeolite structure collapsed after 900 °C aging [31], thus significantly altering the active sites in the catalyst. The results of the experiments and simulations for the 50 and 75% NO_2/NO_x cases are shown in Fig. 9c and d, respectively. The aging factor for the NO_2 SCR reaction needed to be further lowered, as described above, but at the same time, the conversion of NO_x is quite high for the 75% NO_2 case (Fig. 9d), for example close to 100% at 300 °C. However, note that there is a very large N_2O production significantly contributing to the NO_x conversion. When initially exposing the catalyst to the reaction mixture at 150 °C, the ammonium nitrate formation was under-predicted by the model. However, in general, the updated model described the experimental features adequately.

5. Conclusions

In this study a kinetic model for describing the hydrothermal aging of Cu-zeolites used for ammonia SCR has been developed. The catalyst was hydrothermally degreened and aged at 500, 600, 700, 800 and 900 °C. A broad range of experimental conditions were used in the model development, including ammonia storage and release, NH_3 oxidation, NO oxidation and SCR with a different NO_2 to NO_x ratio (0, 50 and 75%). In addition, a model for N_2O production was developed in order to capture large N_2O production at low temperature, which was decreased at medium temperatures and thereafter increased again at high temperatures. This was done by adding two N_2O mechanisms, one at low temperature associated with ammonium nitrate complex formation and one direct route at high temperature.

The effect of aging on the ammonia adsorption and desorption was modeled using NH_3 TPD experiments. The heat of adsorption of ammonia after degreening and aging was determined using micro-calorimeter experiments and the retrieved values were used in the model. The model predicted the TPD experiments well, showing that the use of micro-calorimeter data in kinetic modeling worked well.

The next step was to simulate the aging of the ammonia and NO oxidation reactions. To accomplish this, an aging factor method was developed. In an earlier study, we proposed that ammonia and NO oxidation is occurring on over-exchanged copper sites, while the SCR reaction is faster on the low and medium exchanged sites. As a result, in this study, we propose two aging factors; Factor 1 related to the over-exchanged sites and Factor 2 to the under-exchanged sites. The pre-exponential factors were then multiplied by either of these two aging factors. Factor 1 was used for NO and NH_3 oxidation, and when using this approach, the model could describe the experimental findings well after degreening/aging at 500, 600, 700 and 800 °C. However, after 900 °C different aging factors for NO and ammonia oxidation were needed, but this was not surprising since after this aging, the zeolite structure according to XRD was collapsed.

The SCR reactions were unaffected after 600 °C aging, whereas both NO and ammonia oxidation were affected, something that further supports the theory that different sites age differently. Since no aging was observed for SCR after aging at 600 °C, this case was not modeled. At 700 °C, aging was observed and the aging factor model developed worked well. In addition, this method was also used after 800 °C aging but did not show an adequate description for the entire temperature interval. Not even retuning the activation barrier of the standard SCR reaction gave an appropriate agreement. Earlier UV–vis results had shown that after hydro-thermal aging at high temperature the copper species changed from copper hydroxyls to copper oxides. We propose that after aging at 800 °C, both copper hydroxyls as well as copper oxide sites are available in the catalyst. We therefore add an extra reaction responsible for the SCR on copper oxides and this resulted in a model that could describe the experimental findings well. The results from the model also suggest that the standard SCR reaction is more deactivated during aging compared to SCR with NO_2 present in the feed. In addition, the fast and NO_2 SCR reaction did not possess the same aging characteristic, however the analysis if further complicated due to large ammonium nitrate formation for the case with high NO_2 content.

For the 900 °C aging case, several pre-exponential factors needed to be retuned, due to that the BEA structure had collapsed and the active sites were no longer ion-exchanged copper in a BEA structure. These modeling results, clearly show how complex the hydro thermal aging is over copper zeolites.

Acknowledgements

This study was performed within the Competence Center for Catalysis, Chemical Engineering at Chalmers University and Cummins Inc. The financial support from Cummins Inc. and the Swedish Foundation for Strategic Research (F06-0006) are gratefully acknowledged.

References

[1] I. Nova, L. Lietti, E. Tronconi, P. Forzatti, Chem. Eng. Sci. 56 (2001) 1229–1237.
[2] B. Roduit, A. Wokaun, A. Baiker, Ind. Eng. Chem. Res. 37 (1998) 4577–4590.
[3] J.A. Dumesic, N.-Y. Topsoe, H. Topsoe, Y. Chen, T. Slabiak, J. Catal. 163 (1996) 409–417.
[4] L. Lietti, I. Nova, E. Tronconi, P. Forzatti, Catal. Today 45 (1998).
[5] D. Chatterjee, T. Burkhardt, M. Weibel, E. Tronconi, I. Nova, C. Ciardelli, SAE 2006-01-0468, 2006.
[6] H. Sjövall, L. Olsson, E. Fridell, R.J. Blint, Appl. Catal. B 64 (2006) 180.
[7] H. Sjövall, E. Fridell, R.J. Blint, L. Olsson, Top. Catal. 42–43 (2007) 113–117.
[8] J.-H. Park, H.J. Park, J.H. Baik, I.-S. Nam, C.-H. Shin, J.-H. Lee, B.K. Cho, S.H. Oh, J. Catal. 240 (2006) 47–57.
[9] S. Kieger, G. Delahay, B. Coq, B. Neveu, J. Catal. 183 (1999) 267–280.
[10] J.A. Sullivan, J. Cunningham, M.A. Morris, K. Keneavey, Appl. Catal. B: Environ. 7 (1995) 137–151.
[11] K. Rahkamaa-Tolonen, T. Maunula, M. Lomma, M. Huuhtanen, R.L. Keiski, Catal. Today 100 (2005) 217–222.
[12] A. Pant, S.J. Schmieg, Ind. Eng. Chem. Res. 50 (2011) 5490–5498.
[13] A. Grossale, I. Nova, E. Tronconi, D. Chatterjee, M. Weibel, Top. Catal. 52 (2009) 1837–1841.
[14] P.S. Metkar, V. Balakotaiah, M.P. Harold, Catal. Today 184 (2012) 115–128.
[15] S. Malmberg, M. Votsmeier, J. Gieshoff, N. Söger, L. Mußmann, A. Schuler, A. Drochner, Top. Catal. 42–43 (2007) 33–36.
[16] D. Chatterjee, T. Burkhardt, M. Weibel, I. Nova, A. Grossale, E. Tronconi, SAE 2007-01-1136, 2007.
[17] H. Sjovall, R.J. Blint, A. Gopinath, L. Olsson, Ind. Eng. Chem. Res. 49 (2010) 39–52.
[18] K. Kamasamudram, N.W. Currier, X. Chen, A. Yezerets, Catal. Today 151 (2010) 212–222.
[19] N. Wilken, K. Wijayanti, K. Kamasamudram, N.W. Currier, R. Vedaiyan, A. Yezerets, L. Olsson, Appl. Catal. B 111 (2012) 58.
[20] G. Delahay, S. Kieger, N. Tanchoux, P. Trens, B. Coq, Appl. Catal. B: Environ. 52 (2004) 251–257.
[21] L. Olsson, H. Sjovall, R.J. Blint, Appl. Catal. B 81 (2008) 203–217.
[22] L. Olsson, H. Sjövall, R.J. Blint, Appl. Catal. B: Environ. 87 (2009) 200.
[23] H. Sjövall, R.J. Blint, L. Olsson, Appl. Catal. B 92 (2009) 138.
[24] H. Sjövall, L. Olsson, R.J. Blint, J. Phys. Chem. C 113 (2009) 1393.
[25] N. Wilken, K. Kamasamudram, N.W. Currier, J. Li, A. Yezerets, L. Olsson, Catal. Today 151 (2010) 237.
[26] A. Delabie, K. Pierloot, M.H. Groothaert, B.M. Weckhuysen, A. Schoonheydt, Microporous Mesoporous Mater. 27 (2000) 209–222.
[27] L. Wang, W. Li, G.S. Qi, D. Weng, J. Catal. 289 (2012) 21–29.
[28] S.J. Schmieg, S.H. Oh, C.H. Kim, D.B. Brown, J.H. Lee, C.H.F. Peden, D.H. Kim, Catal. Today 184 (2012) 252–261.
[29] S. Brandenberger, O. Krocher, A. Tissler, R. Althoff, Ind. Eng. Chem. Res. 50 (2011) 4308–4319.
[30] J. Li, N. Wilken, K. Kamasamudram, N.W. Currier, L. Olsson, A. Yezerets, Top. Catal. 56 (2013) 201.
[31] N. Wilken, R. Nedyalkova, K. Kamasamudram, J. Li, N.W. Currier, R. Vedaiyan, A. Yezerets, L. Olsson, Top. Catal. 56 (2013) 317.
[32] S. Shwan, J. Jansson, J. Korsgren, L. Olsson, M. Skoglundh, Catal. Today 197 (2012) 24–37.
[33] S. Shwan, R. Nedyalkova, J. Jansson, J. Korsgren, L. Olsson, M. Skoglundh, Top. Catal. 56 (2013) 80–88.
[34] M. Iwasaki, K. Yamazaki, H. Shinjoh, Appl. Catal. B: Environ. 102 (2011) 302–309.
[35] S.J. Schmieg, S.H. Oh, C.H. Kim, D.B. Brown, J.H. Lee, C.H.F. Peden, D.H. Kim, Catal. Today 184 (2012) 252.
[36] Y.S. Cheng, J. Hoard, C. Lambert, J.H. Kwak, C.H.F. Peden, Catal. Today 136 (2008) 34–39.
[37] S.A. Stevenson, J.C. Vartuli, C.F. Brooks, J. Catal. 190 (2000) 228–239.
[38] M. Colombo, I. Nova, E. Tronconi, V. Schmeisser, B. Bandl-Konrad, L. Zimmermann, Appl. Catal. B: Environ. 111 (2012) 106–118.
[39] J.H. Baik, S.D. Yim, I.S. Nam, Y.S. Mok, J.H. Lee, B.K. Cho, S.H. Oh, Ind. Eng. Chem. Res. 45 (2006) 5258–5267.
[40] P.S. Metkar, M.P. Harold, V. Balakotaiah, Chem. Eng. Sci. 87 (2013) 51–66.
[41] M. Colombo, I. Nova, E. Tronconi, Catal. Today 197 (2012) 243–255.
[42] AVL BOOST Aftertreatment Manual, AVL, 2009 http://www.avl.com
[43] M. Colombo, I. Nova, E. Tronconi, Catal. Today 151 (2010) 223–230.
[44] E. Tronconi, I. Nova, C. Ciardelli, D. Chatterjee, B. Bandl-Konrad, T. Burkhardt, Catal. Today 105 (2005) 529–536.
[45] M. Boudart, G. Djega-Mariadassou, Kinetics of Heterogeneous Catalytic Reactions, Princeton University Press, 1984.
[46] M. Colombo, G. Koltsakis, I. Nova, E. Tronconi, Catal. Today 188 (2012) 42–52.
[47] S.A. Skarlis, D. Berthout, A. Nicolle, C. Dujardin, P. Granger, J. Phys. Chem. C 117 (2013) 7154–7169.
[48] D. Wang, L. Zhang, K. Kamasamudram, W.S. Epling, ACS Catal. 3 (2013) 871–881.
[49] H.Y. Zhu, J.H. Kwak, C.H.F. Peden, J. Szanyi, Catal. Today 205 (2013) 16–23.
[50] O. Mihai, C. Widyastuti, S. Andonova, K. Kamasamudram, J. Li, S. Joshi, N.W. Currier, A. Yezerets, L. Olsson, J. Catal. 311 (2014) 170.
[51] O. Mihai, C.R. Widyastuti, A. Kumar, J. Li, S.Y. Joshi, K. Kamasamudram, N.W. Currier, A. Yezerets, L. Olsson, Catal. Lett. 144 (1) (2014) 70.
[52] G. Delahay, B. Coq, S. Kieger, B. Neveu, Catal. Today 54 (1999) 431.
[53] C. Ciardelli, I. Nova, E. Tronconi, D. Chatterjee, B. Bandl-Konrad, M. Weibel, B. Krutzsch, Appl. Catal. B: Environ. 70 (2007) 80–90.
[54] T.C. Watling, M.R. Ravenscroft, G. Avery, Catal. Today 188 (2012) 32.
[55] B. Pereda-Ayo, U. De La Torre, M.J. Illan-Gomez, A. Bueno-Lopez, J.R. Gonzalez-Velasco, Appl. Catal. B: Environ. 147 (2014) 420–428.
[56] S. Suarez, J.A. Martin, M. Yates, R. Avila, J. Blanco, J. Catal. 229 (2005) 227–236.
[57] Y.J. Kim, J.K. Lee, K.M. Min, S.B. Hong, I.S. Nam, B.K. Cho, J. Catal. 311 (2014) 447–457.
[58] J. Pasel, P. Kassner, B. Montanari, M. Gazzano, A. Vaccari, W. Makowski, T. Lojewski, R. Dziembaj, H. Papp, Appl. Catal. B: Environ. 18 (1998) 199–213.
[59] G.Y. Xie, Z.Y. Liu, Z.P. Zhu, Q.Y. Liu, J. Ge, Z.G. Huang, J. Catal. 224 (2004) 36–41.